2013

Carbon monoxide adsorption on platinum-osmium and platinum-ruthenium-osmium mixed nanoparticles

Nicholas Dimakis

Nestor E. Navarro

Eugene S. Smotkin
Northeastern University

Carbon monoxide adsorption on platinum-osmium and platinum-ruthenium-osmium mixed nanoparticles

Nicholas Dimakis,[1,a)] Nestor E. Navarro,[1] and Eugene S. Smotkin[2]
[1]*Department of Physics and Geology, University of Texas-Pan American, Edinburg, Texas 78539, USA*
[2]*Department of Chemistry and Chemical Biology, Northeastern University, Boston, Massachusetts 02115-5000, USA*

(Received 13 February 2013; accepted 10 April 2013; published online 2 May 2013)

Density functional calculations (DFT) on carbon monoxide (CO) adsorbed on platinum, platinum-osmium, and platinum-ruthenium-osmium nanoclusters are used to elucidate changes on the adsorbate internal bond and the carbon-metal bond, as platinum is alloyed with osmium and ruthenium atoms. The relative strengths of the adsorbate internal bond and the carbon-metal bond upon alloying, which are related to the DFT calculated C–O and C–Pt stretching frequencies, respectively, cannot be explained by the traditional 5σ-donation/$2\pi^*$-back-donation theoretical model. Using a modified π-attraction σ-repulsion mechanism, we ascribe the strength of the CO adsorbate internal bond to changes in the polarization of the adsorbate-substrate hybrid orbitals towards carbon. The strength of the carbon-metal bond is quantitatively related to the CO contribution to the adsorbate-substrate hybrid orbitals and the *sp* and *d* populations of adsorbing platinum atom. This work complements prior work on corresponding slabs using periodic DFT. Similarities and differences between cluster and periodic DFT calculations are discussed. © *2013 AIP Publishing LLC*. [http://dx.doi.org/10.1063/1.4802817]

I. INTRODUCTION

Platinum based alloys serve as anode catalysts for direct oxidation methanol fuel cells (DMFC).[1–14] These catalysts typically contain Ru, Os, Ir, and Sn atoms as alloying elements for binary (e.g., PtRu,[15,16] PtSn[17,18]), tertiary (e.g., PtRuOs[19]), and quaternary (e.g., PtRuOsIr[13]) Pt-based alloys. As methanol is oxidized on the surface of the DMFC anode catalyst, carbon monoxide, an intermediate in the oxidation reaction, is strongly adsorbed on the catalyst surface (CO_{ads}). The CO_{ads} blocks the Pt active sites, thus reducing the efficiency of the anode catalyst.[20,21] In the past, PtRu alloys have been found to have an improved electrocatalytical activity relative to pure Pt.[22–24] However, PtOs[25–29] alloys may replace PtRu alloys, due to their higher catalytic activity for DMFC operation relative to PtRu and PtSn alloys. Still, the effect of CO adsorption on binary PtOs and tertiary PtRuOs alloys is poorly understood.

Adsorbed CO serves as a probe for the electronic structure of Pt-based anode catalysts. As CO is adsorbed on pure metals and alloys its stretching frequency (ν_{CO}) monitored by modulated infrared absorption spectroscopy (PM-IRAS) reduces relative to free CO.[19] This effect has been interpreted as weakening of the adsorbate internal C–O bond (CO_{ads} internal bond).[30] At low CO coverage, CO is adsorbed at the atop and bridge configurations for ultrahigh vacuum and aqueous electrochemical interface environments, respectively.[31–33] Moreover, PM-IRAS for CO/PtRu, CO/PtOs, and CO/PtRuOs[19] and scanning tunneling microscopy for CO/PtCo[34] show that CO is exclusively adsorbed on the Pt site of the Pt-based alloy under low CO coverage. Potential- and coverage-dependent PM-IRAS of CO adsorbed on single-phase polycrystalline arc-melted PtOs and PtRuOs alloy electrodes was employed by Liu *et al.*[19] to observe ν_{CO} reduction following the substrate trend PtRuOs(65/25/10) > PtRuOs(8/1/1) > PtOs(8/2) > Pt at 0.1% CO coverage. Density functional theory (DFT) on small Pt and PtOs nanoparticles was used by Ishikawa *et al.*[20] to observe ν_{CO}, C–Pt stretching frequency (ν_{CPt}), and CO_{ads} enthalpy of adsorption (E_{ads}) reductions upon Pt alloying with Os. Recently, Dimakis *et al.*[35] using periodic DFT for CO_{ads} on $PtOs_2$ and $PtOs_4$ binary alloys and the on the tertiary $PtRu_2Os_2$ alloy observed CO_{ads} internal bond and adsorbate-metal bond (C–Pt bond) strengthening following the substrate trends of $PtOs_4$ > Pt > $PtOs_2$ > $PtRu_2Os_2$ and Pt > $PtOs_4$ > $PtOs_2$ > $PtRu_2Os_2$, respectively. However, the importance of the work of Dimakis *et al.*[35] was the theoretical interpretation of the above trends using charges and polarizations of adsorbate-substrate hybrid orbitals. Their work was based on a modified π-attraction σ-repulsion mechanism, with the inclusion of the σ-attractive part via charge donation to the substrate (vide infra).

The first theoretical interpretation of the weakening of the CO_{ads} internal bond relative to free CO is attributed to Blyholder.[36] In his original work, the weakening of the CO_{ads} internal bond was ascribed to charge variations of the entire adsorbate π-system, whereas the CO_{ads} σ-type bonds were assumed constant. Later, Bagus and Pacchioni[37] reformed Blyholder's original interpretation by only considering the effect of the 5σ and $2\pi^*$ CO frontier molecular orbitals (MOs) and their interactions with the substrate metal d-bands as $5\sigma \rightarrow d_{z^2}$ (5σ-donation) and $d_{xz,\,yz} \rightarrow 2\pi^*$ ($2\pi^*$-back

a)Author to whom correspondence should be addressed. Electronic mail: dimakis@utpa.edu

donation). However, the 5σ-donation/$2\pi^*$-back donation mechanism proposed by Bagus and Pacchioni[37] (frontier orbital model) is the phenomenological model that appears in the literature as the "Blyholder model," which is different than the one originally described by Blyholder.[36] In the frontier orbital model, the depletion of the 5σ C–O anti-bonding MO strengthens the CO_{ads} internal bond, whereas populating the $2\pi^*$ MO weakens the CO_{ads} internal bond (also a C–O anti-bonding MO). Both processes contribute to the formation of a stable carbon-metal bond. Although the frontier orbital model successfully explained CO adsorption on pure metals (e.g., CO/Ni, CO/Fe, CO/Cr, and CO/Ti)[38] it failed to explain changes on C–Pt bonding as Pt was alloyed with Ru atoms.[39]

Hammer and Nørskov[40] in their report on the nobleness of gold they correlated dissociation energies for H_2 adsorbed on Cu, Ni, Pt, and Au with the orbital overlap between the substrate and the H_2 adsorbate. Later Hammer *et al.*[41] in their report on CO adsorption on metal and alloy surfaces they used the frontier orbital model to correlate CO E_{ads} reduction with the downshift in energy of the substrate d-band center (e_d). The e_d downshift is indicative of stronger CO_{ads} internal bond through reduced overlap of the unperturbed $2\pi^*$ CO MO with the substrate d-band. Nilsson *et al.*,[42] Bennich *et al.*,[43] and Föhlisch *et al.*[44–46] challenged the frontier orbital model by considering π-bonding and σ-repulsion (π-σ model) for surface adsorption. More specifically, the π-σ model considers adsorbate-substrate tilde-type hybrid orbitals instead of the frontier CO MOs of the frontier orbital model. Their theory is based on experimentally measuring the electronic structure of N_2 and CO molecules adsorbed on Ni (100) and Cu (100) surfaces by using x-ray emission spectroscopy (XES) and by quantum mechanical calculations. In the original π-σ model, the adsorbate-substrate π-bonding is ascribed to the tilde-type orbitals $1\tilde{\pi}$, $\tilde{d}_\pi$, and $2\tilde{\pi}^*$, where the $\tilde{d}_\pi$ orbital is a hybrid of the unperturbed 1π and $2\pi^*$ CO MOs mixed with the metal $d_{xz,\,yz}$-band. For the $\tilde{\pi}$-system charge exchange is observed between the CO and the metal substrate $d_{xz,\,yz}$-band, accompanied by polarization within the CO molecule. The CO_{ads} internal bond is weakened due to increased $1\tilde{\pi}$ polarization towards carbon relative to free CO.[47] In contrast to the frontier orbital model, the original π-σ model does not assume direct $2\pi^*$ back-donation from the substrate metal bands to the unperturbed $2\pi^*$CO MO. The overall $\tilde{\pi}$-interaction is bonding to the metal surface.

The σ-repulsion in the original π-σ model is ascribed to $4\tilde{\sigma}$ and $5\tilde{\sigma}$ orbitals and the $\tilde{d}_\sigma$ band. The $\tilde{d}_\sigma$ band is a hybrid of the unperturbed 5σ CO MO and the d_{z^2} substrate band. In the original π-σ model charge reduction was observed in the CO regions of the $4\tilde{\sigma}$ and $5\tilde{\sigma}$ orbitals concomitant with reduction in the d_{z^2} population, which is in contrast to the σ donation of the frontier orbital model. The σ-repulsion is primarily ascribed to charge redistribution within the CO molecule,[45] which diminishes the weakening of the CO_{ads} internal bond due to the changes in the $\tilde{\pi}$-system. The $\tilde{\sigma}$-system minimizes C–Pt bonding, which is caused by the $\tilde{\pi}$-attractive interaction. However, Dimakis *et al.*[39] showed that the $\tilde{\sigma}$-system contains both attractive (through evidence of charge donation to the substrate) and repulsive components (vide infra). The observations of Dimakis *et al.*[39] are in agreement with quantum mechanical calculations by Kresse *et al.*[48] on CO/Pt(111), where the importance of the 5σ donation was addressed. Moreover, the partial occupancy of the $\tilde{d}_\sigma$ band, as verified by Rangelov *et al.*[49] using inverse photoemission spectra on CO adsorbed on Ni, Pd, and Pt surfaces and by Aizawa and Tsuneyuki[50] using periodic plane wave DFT calculations on CO/Pt(111), is also indicative of σ donation to the substrate bands.

This work complements our prior work on CO_{ads} on binary $PtOs_2$ and $PtOs_4$ alloys and on the $PtRu_2Os_2$ tertiary alloy using periodic DFT,[35] where the variations on the CO_{ads} and C–Pt bonds were correlated with changes in the populations of the carbon $2s$ and p_{xy} atomic orbitals, as well as the s, p, and d orbitals of the adsorbing Pt atom (Pt^c). Here, we study the validity of our last model by examining the CO adsorption on Pt_{26}, $Pt_{24}Os_2$, $Pt_{22}Os_4$, and $Pt_{22}Ru_2Os_2$ nanoclusters, where the nanocluster structure mostly corresponds to the slab structure priory explored by periodic DFT. Moreover, the C–Pt bond strength is quantitatively correlated with the CO contributions to the adsorbate $\tilde{\sigma}$ and $\tilde{\pi}$ orbitals and the s, p, d atomic populations of the Pt^c. In accordance with our prior reports, we consider all hybrid orbitals from energies as low as the $4\tilde{\sigma}$ to as high as the $2\tilde{\pi}^*$.

II. MODELS AND COMPUTATIONAL METHODS

Our computational strategy is similar to the one previously presented.[39] The mixed nanoparticles were modeled by the three layer Pt_{26} nanocluster as (13)(12)(1) layer configuration, with a lattice parameter of 3.924 Å. The alloy nanoclusters were constructed by placing Ru and Os atoms at the nearest neighbor sites on the adsorbing face. Moreover, a single CO molecule was adsorbed at the atop configuration (Fig. 1). The cluster configurations used here are adequate for modeling the effect of single atop CO chemisorption on Pt and Pt-based alloy surfaces, as previously reported.[30] Unrestricted DFT[51–53] on CO/$Pt_{26-n}Os_n$, $n = 0$, 2, 4 nanoclusters and the CO/$Pt_{22}Ru_2Os_2$ nanocluster was used for the calculation of the fractional C–O and C–Pt geometries and the corresponding vibrational frequencies ν_{CO} and ν_{CPt}, the appropriate Fermi levels, and the $E_{ads.}$ The hybrid X3LYP[54,55] functional was employed here, which is an extension to the commonly-used B3LYP[56] functional and provides more accurate heats of formation.[57] A triple-ζ basis set is used here. More specifically, the Pt, Ru, and Os heavy atom wave functions are described by the effective core LACV3P**++ basis set. This basis set includes valence and outermost core electrons, polarization,[58] and diffuse[59] basis set functions (denoted by "**" and "++," respectively). The $5s^25p^65d^96s^1$, $4s^24p^64d^75s^1$, and $5s^25p^65d^66s^2$ "valence"[60] configuration are used for Pt, Ru, and Os atoms, respectively. The remaining core electrons are treated with effective core potentials (ECP),[61] which accounts for mass-velocity and Darwin relativistic corrections. The all-electron 6-311G**++ Pople basis set is used for carbon and oxygen atoms.[62] The selection of the triple-ζ basis sets minimizes[63] the basis set superposition error (BSSE),[64] thus providing more accurate E_{ads}. DFT calculations are performed using Jaguar 7.6,[65] which incorporates the pseudospectral method[66–71] to calculate most of the fundamental time-consuming integrals with the same

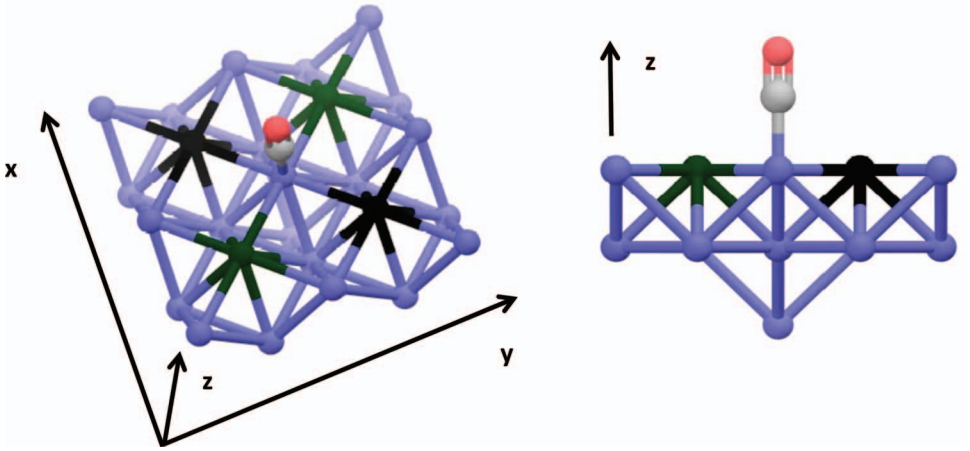

FIG. 1. The CO/$Pt_{22}Ru_2Os_2$ nanocluster. Ru atoms are depicted in black and Os atoms in green.

accuracy as the fully analytical DFT codes. For each nanocluster used here, the ground state multiplicity is determined through a series of SCF energy calculations for various spin multiplicity values (vide infra).[30] Consequently, the spin-optimized cluster is geometrically optimized by letting the CO molecule to relax, while all metal atoms remain locked to the original positions. As was explained previously,[39] this process is necessary in order to avoid gross cluster relaxation, which would not be characteristic of the periodic lattice structure we aim to model. The ν_{CO} and ν_{CPt} are computed by using the partial Hessian approach for C, O, and Pt^c, which conserves CPU time, and thus avoiding the unnecessary calculation of cluster metal-metal normal mode vibrations. The Pt, Ru, and Os electron populations are calculated using the Natural Bond Order (NBO)[72] program. NBO calculates, among others, atomic electron populations (per angular momentum). Density-of-states (DOS) and overlap population DOS (OPDOS) are calculated using the AOMIX program.[63,73] AOMIX at its latest version processes output files from a variety of quantum mechanical packages and generates DOS and OPDOS spectra in terms of constituent chemical fragments. The cluster calculation Fermi levels are the lowest of the quantity (E_{HOMO} + E_{LUMO})/2 for either alpha or beta electrons.

III. RESULTS AND DISCUSSION

A. Pt alloying with Ru/Os atoms-clean substrates

As Pt is alloyed with Ru/Os atoms in the nearest neighbor sites of the adsorbing atom (Fig. 1), the Os electronic configuration becomes $s^{0.81}p^{0.06}d^{6.80}$, $s^{0.81}p^{0.06}d^{6.82}$, and $s^{0.82}p^{0.07}d^{6.83}$ for $Pt_{24}Os_2$, $Pt_{22}Os_4$, and $Pt_{22}Ru_2Os_2$, respectively (the electronic configuration for atomic Os is s^2d^6). Similarly, the Ru electronic configuration for the $Pt_{22}Ru_2Os_2$ nanocluster is $s^{0.57}p^{0.05}d^{7.07}$ (the electronic configuration for atomic Ru is s^1d^7). The alloying effect on the $Pt_{24}Os_2$ nanocluster causes substantial electron depletion of the osmium *sp* orbital by about 1.13 *e*/atom and increase of the osmium *d* orbital population by 0.8 *e*/atom. These effects increase the overall Pt^c-*s* and -*p* orbital population by about 0.1 *e*, whereas the Pt^c-*d* orbital population remains constant. The Pt^c-*s*, -*p*, and -*d* orbital populations for Pt_{26}, $Pt_{24}Os_2$, $Pt_{22}Os_4$, and $Pt_{22}Ru_2Os_2$ nanoclusters are shown in Table I. The increase on the Pt^c-*sp* orbital population is along with the increase of the Os mole percent, which in turn is indicative of increased σ-type repulsion between carbon and Pt^c upon CO adsorption (vide infra). Concomitantly, for all other Pt atoms of the nanocluster a decrease in their *sp* orbital population is accompanied by increases in their d orbital population. Moreover, the Ru and Os alloying on the $Pt_{22}Ru_2Os_2$ nanocluster cause a depletion of the ruthenium *sp* orbital by 0.38 *e*/atom and a small increase in this atom *d* orbital population by 0.07 *e*/atom. However, the presence of the ruthenium atoms in the $Pt_{22}Ru_2Os_2$ nanocluster reduce the Pt^c-*sp* orbital population by about 0.02 *e*

TABLE I. CO contributions to the adsorbate $4\tilde{\sigma}$, $5\tilde{\sigma}$, $1\tilde{\pi}$, $\tilde{d}_\pi$, $\tilde{d}_\sigma$, the occupied part of the $2\tilde{\pi}^*$ orbitals, and the Pt^c-*s*, -*p*, and -*d* orbitals for CO/Pt_{26}, CO/$Pt_{24}Os_2$, CO/$Pt_{22}Os_4$, and CO/$Pt_{22}Ru_2Os_2$ nanoclusters. The CO contributions are calculated by DOS spectrum integration at appropriate energy ranges. The Pt orbital populations are calculated by the NBO program. The values in parenthesis refer to corresponding populations for clean substrates.

Molecule/atom	Orbital	CO/Pt_{26}	CO/$Pt_{24}Os_2$	CO/$Pt_{22}Os_4$	CO/$Pt_{22}Ru_2Os_2$
CO	$4\tilde{\sigma}$	1.50	1.51	1.50	1.51
	$5\tilde{\sigma}$	1.54	1.52	1.54	1.54
	$\tilde{d}_\sigma$	0.30	0.29	0.29	0.32
	$1\tilde{\pi}$	3.55	3.55	3.52	3.51
	$\tilde{d}_\pi$	0.36	0.37	0.38	0.41
	$2\tilde{\pi}^*$	0.51	0.52	0.50	0.51
Pt^c	6*s*	0.80	0.80	0.83	0.82
		(0.88)	(0.97)	(0.99)	(1.00)
	6*p*	0.04	0.06	0.07	<0.01
		(0.03)	(0.04)	(0.04)	(<0.01)
	$5d_{z^2}$	1.58	1.58	1.62	1.63
		(1.91)	(1.91)	(1.90)	(1.91)
	$5d_{xz}$[a]	1.84	1.83	1.83	1.82
		(1.86)	(1.85)	(1.87)	(1.86)
	$5d_{xy}$[b]	1.93	1.93	1.90	1.91
		(1.82)	(1.82)	(1.82)	(1.81)
	5*d*	9.11	9.10	9.07	9.08
		(9.26)	(9.26)	(9.26)	(9.26)

[a]Average values $(5d_{xz} + 5d_{yz})/2$.
[b]$(5d_{xy} + 5d_{x^2-y^2})/2$ are assumed.

relative to $Pt_{22}Os_4$. The reduction of the Pt^c-*sp* orbital population is indicative of reduced σ-type repulsion and is along with the ν_{CPt} increase for $CO/Pt_{22}Ru_2Os_2$ relative to $CO/Pt_{22}Os_4$. A table of the partial charges per *sp* and *d* orbitals for the clean substrates Pt_{26}, $Pt_{24}Os_2$, $Pt_{22}Os_4$, and $Pt_{22}Ru_2Os_2$ is provided as supplementary material.

B. C–O and C–Pt optimal geometries, corresponding vibrational frequencies, and E_{ads}

Table II shows the C–O and C–Pt optimal geometries, the corresponding vibrational frequencies ν_{CO} and ν_{CPt}, and the E_{ads} for CO_{ads} on Pt_{26}, $Pt_{24}Os_2$, $Pt_{22}Os_4$, and $Pt_{22}Ru_2Os_2$ nanoclusters in the arrangement of Figure 1. Moreover, Table II also provides the Fermi levels for the above clusters with and without an adsorbed CO. The DFT optimized C–O and C–Pt bond lengths for CO_{ads} on $Pt_{24}Os_2$ and $Pt_{22}Os_4$ nanoclusters are within the ranges of the corresponding bond lengths reported by Ishikawa *et al.*[20] for CO_{ads} on the (111) two-layer clusters $(Pt_3)(Os_2Pt_5)$ and $(Pt_3)(Os_4Pt_3)$. The DFT computed frequencies ν_{CO} and ν_{CPt} are systematically overestimated by DFT. For some functionals paired with appropriate basis sets scaling factors can be applied on the DFT computed vibrational frequencies for quantitative comparison with corresponding experimental observations.[74] However, these parameters are still not known for the X3LYP functional paired with the LACV3P**++ basis set used here. As expected, variations on the computed C–O and C–Pt bond lengths follow an inverse relationship with variations on computed ν_{CO} and ν_{CPt}. Moreover, it is also expected that ν_{CPt} reduces along with $|E_{ads}|$. However, for $CO/Pt_{22}Os_4$ relative to $CO/Pt_{22}Ru_2Os_2$ the ν_{CPt} is increased by 4 cm^{-1} accompanied by 0.12 eV E_{ads} reduction (Table II). This effect has been previously reported by Koper *et al.* for CO_{ads} on Pt-Ru alloys.[75] It is attributed to the fact that ν_{CPt} and E_{ads} are derived from a local and global property of the potential energy surface, respectively, and thus in some cases vibrational spectroscopy measurements are difficult to interpret.

The weakening of the CO_{ads} internal bond and the C–Pt surface bond for CO_{ads} on $Pt_{24}Os_2$ relative to Pt_{26}, as evidenced by the corresponding stretching frequency reductions and E_{ads} reduction, are in agreement with previous results on periodic DFT calculations,[35] cluster DFT calculations,[20] and FTIR experimental results.[19] However, calculations here show that as the Os mole percent in the Pt-based alloy increases the CO_{ads} internal bond and the C–Pt surface bond further weaken. This result is in contrast with the prior calculations on DFT periodic slabs, and is due to the different behavior exhibited between nanoparticles and periodic slabs. For example, it was found that platinum nanoparticles are paramagnetic;[30] however, platinum slabs do not exhibit magnetic properties.

TABLE II. Calculated C–O and C–Pt distances and corresponding stretching frequencies ν_{CO}, ν_{CPt}, Fermi energies, E_{ads}, and Pt-e_d d-band centers (relative to corresponding Fermi energies) for the DFT geometrically optimized CO/Pt_{26}, $CO/Pt_{24}Os_2$, $CO/Pt_{22}Os_4$, and $CO/Pt_{22}Ru_2Os_2$ nanoclusters. The values in parenthesis refer to corresponding clean substrates properties.

Property	CO/Pt_{26}	$CO/Pt_{24}Os_2$	$CO/Pt_{22}Os_4$	$CO/Pt_{22}Ru_2Os_2$
d_{C-O} (Å)	1.140	1.141	1.142	1.143
ν_{CO} (cm^{-1})	2260	2190	2183	2178
d_{C-Pt} (Å)	1.845	1.849	1.861	1.857
ν_{CPt} (cm^{-1})	563	528	511	515
E_{Fermi} (eV)	−4.83	−4.76	−4.99	−5.02
	(−4.95)	(−5.06)	(−4.94)	(−5.00)
E_{ads}(eV)	−1.90	−1.80	−1.56	−1.44
Pt-e_d (eV)	−3.12	−3.27	−3.26	−3.29

1. The effect of the nanocluster spin multiplicity on the C–O and C–Pt bond lengths and the corresponding stretching frequencies

The importance of properly selecting the ground state spin multiplicity of a nanocluster was first addressed by Kua and Goddard in their studies of organics chemisorption on Pt,[76] and in transition states involved with methanol oxidation on monolayer model metal surfaces.[77] Figure 2 shows the effect of the spin multiplicity on the SCF conformational energy, the C–O and C–Pt optimized distances, and the corresponding stretching frequencies ν_{CO} and ν_{CPt} for the CO/Pt_{26} nanocluster. For this nanocluster, the ground state corresponds to spin multiplicity 17. Here, DFT partial C–O and C–Pt geometry optimization calculations for spin multiplicities greater than 23 lead to either poor convergence or to conformations with SCF energies higher than the spin-optimized ground state. These observations are also applicable to all nanocluster conformations used in this work, with and without an adsorbed CO. The high multiplicity of the CO/Pt_{26} nanocluster is indicative of the presence of paramagnetic effects for the Pt_{26} substrate, an effect which is not evident when CO is adsorbed on the corresponding Pt periodic slab,[35] mostly due to smearing of the electron density around the Fermi level. For spin multiplicities 9 and 15, Jaguar was trapped into a flat valley-type potential energy surface, and thus the calculated frequencies suffered of numerical instability. Figure 2 shows that, for spin multiplicities 1–23, the variances on the ν_{CO} and ν_{CPt} are 2133–2205 cm^{-1} and 457–530 cm^{-1}, respectively. Therefore, if non-spin optimized cluster calculations are employed the calculated ν_{CO} and ν_{CPt} values may substantially differ from the corresponding values obtained by spin-optimized calculations. For the CO/Pt_{26} nanocluster, the ν_{CO} and ν_{CPt} values obtained through spin optimized and non-spin optimized calculations differ by about 62 cm^{-1} and 31 cm^{-1}, respectively.

2. CO adsorbed on the Pt_{26} nanocluster

The CO adsorption on pure Pt under a modified π-σ model has been explained before.[35,39] It is briefly explained below.

a. $\tilde{\sigma}$-system. In the modified π-σ model of Dimakis *et al.*[35,39] the $\tilde{\sigma}$-system consists of the same tilde-type CO-substrate orbitals as the original π-σ model of Nilsson and coworkers (i.e., the $4\tilde{\sigma}$ and $5\tilde{\sigma}$ orbitals, and the $\tilde{d}_\sigma$-band).[42,44–47] The CO contributions to the $\tilde{\sigma}$ and $\tilde{\pi}$ orbitals as well as the

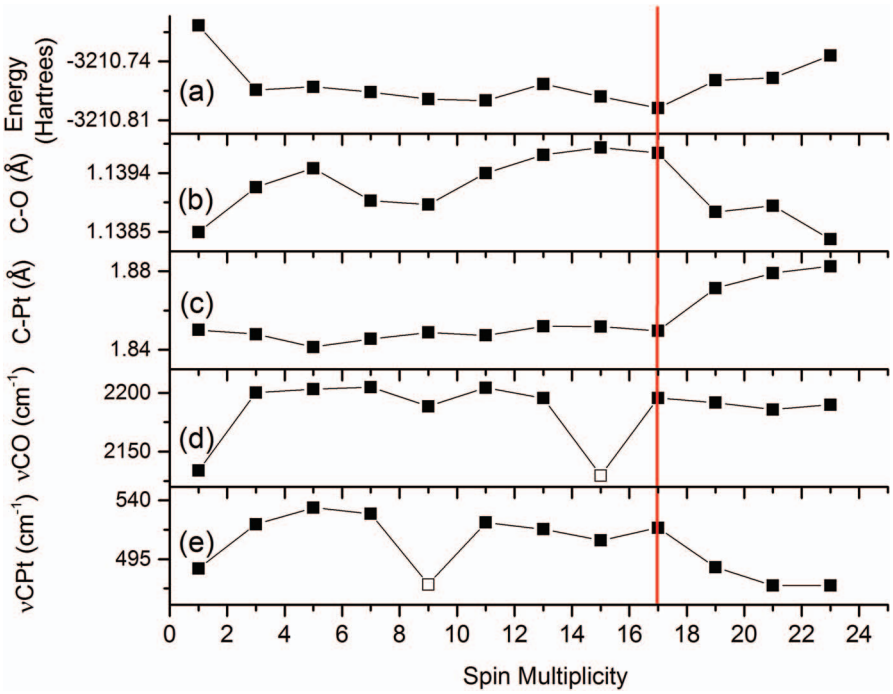

FIG. 2. (a) Conformational SCF energy, (b) C–O, and (c) C–Pt distances and corresponding stretching frequencies ν_{CO} and ν_{CPt} for the CO/Pt_{26} nanocluster at various spin multiplicities. The vertical red line corresponds to the spin optimized ground state. The open squares indicate calculated frequencies, which suffered numerical instability.

Pt^c-*sp* and -*d* orbital populations are shown in Table I. Partial charges for Pt (per layer) and Ru/Os for the clean substrates Pt_{26}, $Pt_{24}Os_2$, $Pt_{22}Os_4$, and $Pt_{22}Ru_2Os_2$ are shown in the supplementary material.[78] In contrast to the original π-σ model, Dimakis *et al.*[39] in their report on CO/Pt and CO/PtRu alloys showed that if adsorption is considered in a step-wise fashion, σ donation concomitant with a reduction of the substrate d_{z^2} population is possible. Figure 3 shows the Pt DOS for CO adsorbed on nanoclusters of this work. During CO adsorption

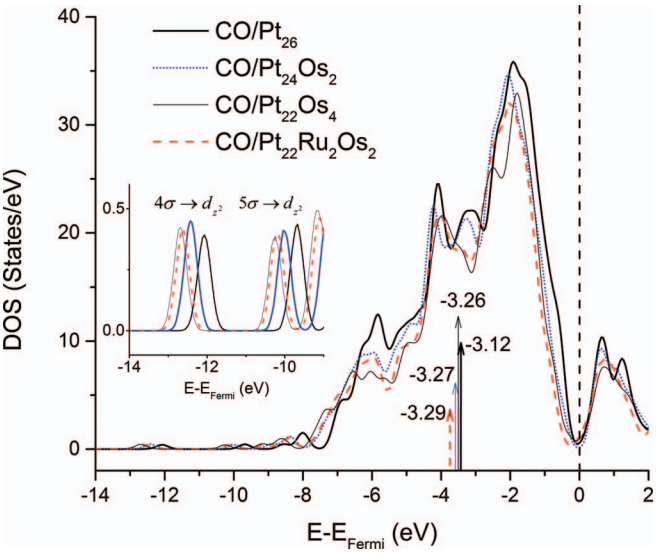

FIG. 3. Pt DOS for CO/Pt_{26}, CO/$Pt_{24}Os_2$, CO/$Pt_{22}Os_4$, and CO/$Pt_{22}Ru_2Os_2$. Vertical arrows show Pt-e_d, whereas the vertical dashed line is the Fermi level. (Inset) The existence of peaks in the d-band DOS spectrum in the energy regions of the $4\tilde{\sigma}$ and $5\tilde{\sigma}$ orbitals verifies the 4σ, $5\sigma \rightarrow d_{z^2}$ donation mechanism.

charge is transferred from the CO region of the $4\tilde{\sigma}$ and $5\tilde{\sigma}$ orbitals to the substrate *sp*- and d_{z^2}-bands, as verified by the $4\tilde{\sigma}$ and $5\tilde{\sigma}$ orbitals' charge reduction in their CO regions relative to free CO (Table I) and the presence of peaks in the lower energy part of the CO-substrate d-band DOS spectra (Fig. 3, inset), respectively. Although Table I shows that the *overall* Pt^c-d_{z^2} population diminishes due to the adsorption process, the parts of the d_{z^2} that are in the energy regions of the $4\tilde{\sigma}$ and $5\tilde{\sigma}$ orbitals' have increased charge. This picture is analogous to the σ donation described by the frontier orbital model, where charge from unperturbed 5σ MO was transferred to the substrate bands, and it applies to all nanoclusters used here.[37] Figures 4 and 5 show the σ and π CO DOS, respectively, for nanoclusters of this work: The CO DOS is factor discomposed into carbon and oxygen atomic contributions. Figure 4 shows a major charge redistribution, which occurs within the CO region of the $4\tilde{\sigma}$ and $5\tilde{\sigma}$ orbitals. More specifically, the $4\tilde{\sigma}$ orbital polarizes towards carbon, while the reverse effect is observed for the $5\tilde{\sigma}$ orbital. These polarizations directions are exactly opposite to what are observed for the 4σ and 5σ MOs of the free CO. Moreover, the $\tilde{d}_{\sigma}$-band polarizes towards carbon (Figure 4). For the $4\tilde{\sigma}$ and $5\tilde{\sigma}$ orbitals, the increase/reduction of their polarization towards carbon is along with the increase/reduction in their carbon 2*s* orbital population. As CO is adsorbed on the substrate, changes in the $4\tilde{\sigma}$ and $5\tilde{\sigma}$ polarizations *alone*, increase the $4\tilde{\sigma}$ C–O anti-bonding character and reduce the $5\tilde{\sigma}$ C–O anti-bonding character relative to their free CO counterparts. Figure 6 shows OPDOS for CO/Pt_{26} and free CO. The C–O OPDOS for the $\tilde{\sigma}$-system reveals that the combined effect of the charge transfer from the CO region of the $4\tilde{\sigma}$ and $5\tilde{\sigma}$ orbitals towards the substrate *and* the above discussed polarization changes reduce

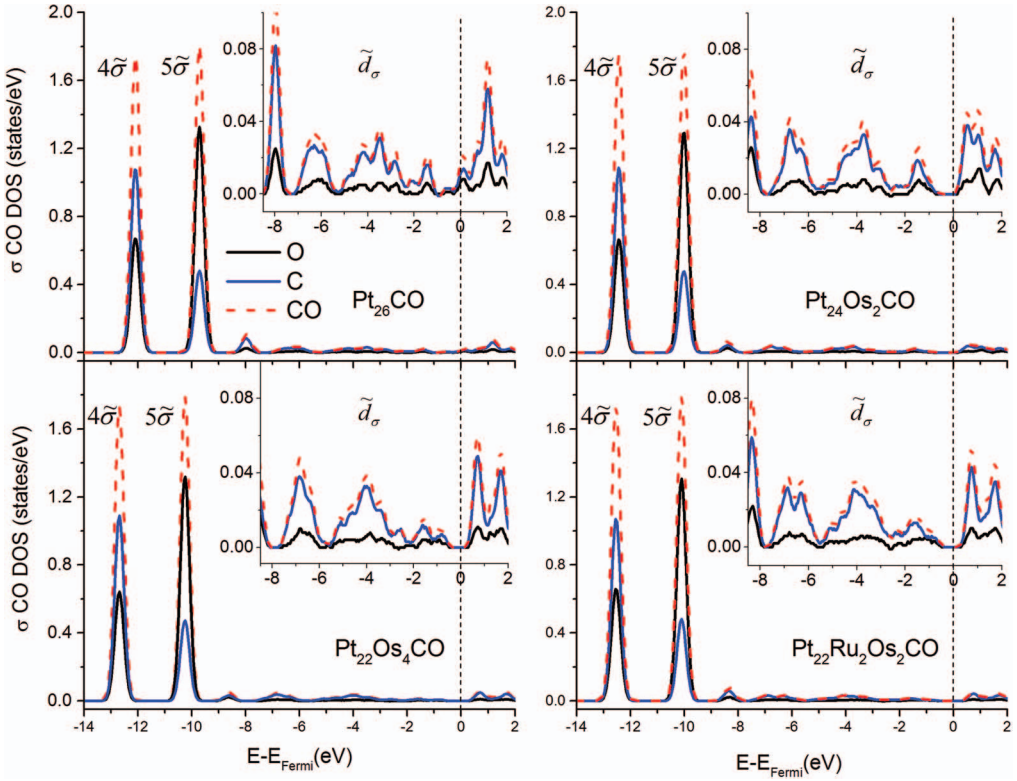

FIG. 4. σ CO DOS for CO/Pt_{26}, CO/$Pt_{24}Os_2$, CO/$Pt_{22}Os_4$, and CO/$Pt_{22}Ru_2Os_2$ nanoclusters as calculated by AOMIX. CO DOS (red dashed line) is factor decomposed into contributions from C (blue solid line) and O (black solid line) atomic orbitals.

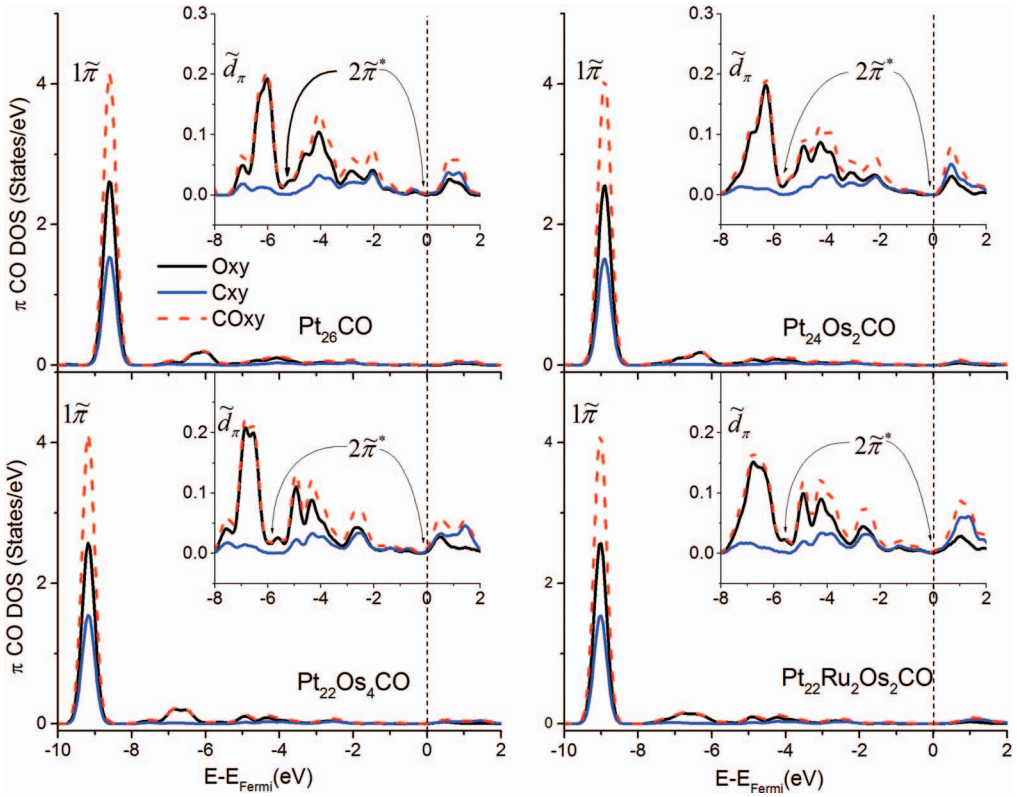

FIG. 5. π CO DOS for CO/Pt_{26}, CO/$Pt_{24}Os_2$, CO/$Pt_{22}Os_4$, and CO/$Pt_{22}Ru_2Os_2$ nanoclusters as calculated by AOMIX. CO DOS (red dashed line) is factor decomposed into contributions from C (blue solid line) and O (black solid line) atomic orbitals.

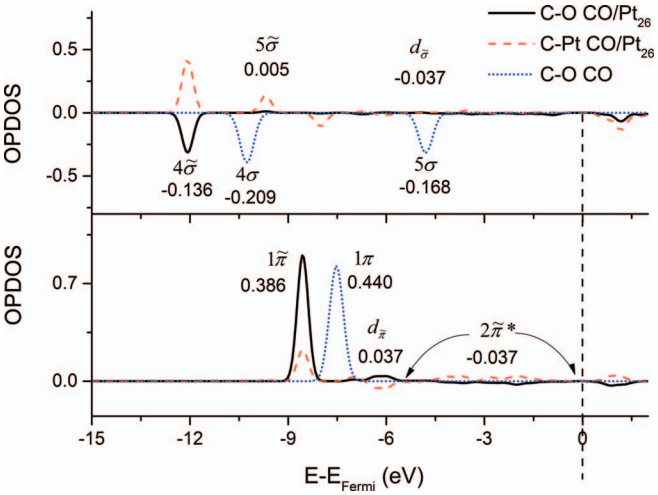

FIG. 6. OPDOS for CO/Pt_{26} and free CO. (Upper graph) $\tilde{\sigma}$-system. (Lower graph) $\tilde{\pi}$-system. Values represent C–O OPDOS. The vertical dash line is the Fermi level.

the $4\tilde{\sigma}$ C–O anti-bonding character and change the $5\tilde{\sigma}$ from anti-bonding in the free CO to nonbonding in the CO/Pt_{26}. Figure 6 verifies that changes in the $\tilde{\sigma}$-system strengthen the CO_{ads} internal bond relative to free CO, in agreement with Föhlisch *et al.*[45] Moreover, the $\tilde{\sigma}$-system is bonding to the metal: The C–Pt bonding caused by the $4\tilde{\sigma}$ and $5\tilde{\sigma}$ orbitals is not counterbalanced by the presence of the C–Pt anti-bonding $\tilde{d}_{\sigma}$-band, due to $\tilde{d}_{\sigma}$-band partial occupancy, which reduces the orbital's C–Pt repulsion.[50] The C–Pt OPDOS shows that the overall effect of the $\tilde{\sigma}$-system as described here is bonding to the substrate ($\tilde{\sigma}$ C–Pt OPDOS for CO/Pt_{26} is about 0.195, Fig. 6, upper graph).

b. $\tilde{\pi}$-system. Consistent with our prior work, the $\tilde{\pi}$-system of the modified π-σ model contains the $1\tilde{\pi}$ orbital, the $\tilde{d}_{\pi}$-band, and the occupied part of the $2\tilde{\pi}^*$-band. The $\tilde{d}_{\pi}$-and $2\tilde{\pi}^*$-bands have mostly metallic character, whereas the $1\tilde{\pi}$ orbital maintains the shape of the 1π CO MO (Figure 4). For the systems examined here, the $\tilde{d}_{\pi}$-band has some C–Pt anti-bonding character (Fig. 6, lower graph). As CO is adsorbed on the Pt_{26} cluster, change is transferred from the CO region of the $1\tilde{\pi}$ orbital towards the metal $d_{xz,\,yz}$ -band. Concomitantly, the $1\tilde{\pi}$ polarization towards oxygen is reduced, leading to increased carbon p_{xy} population relative to the 1π MO of the free CO. The above effects on the $1\tilde{\pi}$ orbital weaken the CO_{ads} internal bond. Moreover, the presence of a partially populated $2\tilde{\pi}^*$-band (C–O anti-bonding) further weakens the C–O bond, while the presence of the $\tilde{d}_{\pi}$-band (C–O bonding, Fig. 6, lower graph) minimizes this weakening. Overall, the $\tilde{\pi}$-system weakens the CO_{ads} internal bond and more than offsets the strengthening caused by the $\tilde{\sigma}$-system. The $\tilde{\pi}$-system is bonding to the substrate.

3. CO adsorbed on the $Pt_{24}Os_2$ nanocluster

a. $\tilde{\sigma}$-system. Table III shows the charge differences in the carbon and oxygen contributions to the $\tilde{\sigma}$- and $\tilde{\pi}$-orbitals for the $CO/Pt_{24}Os_2$, $CO/Pt_{22}Os_4$, and $CO/Pt_{22}Ru_2Os_2$ nanoclusters relative to the CO/Pt_{26} nanocluster. It is evident from Table I that alloying the Pt_{26} nanocluster with Os and Ru/Os atoms, as shown in Figure 1, minimally affects the CO contributions to the $\tilde{\sigma}$- and $\tilde{\pi}$-orbitals. This observation is in agreement with our prior work for CO adsorption on PtOs and $PtRu_2Os_2$ slabs using periodic DFT.[35] For example, for $CO/Pt_{24}Os_2$ relative to CO/Pt_{26} the charges in the CO regions of $4\tilde{\sigma}$ and $5\tilde{\sigma}$ orbitals only change by about 0.01 *e* and 0.02 *e*, respectively. Therefore, for the systems examined here, the origins of the tilde-orbital polarizations are analyzed in detail, thus avoiding premature judgments about their effects on the relative strength of the CO_{ads} and C–Pt bonds. Moreover, when available, C–O and C–Pt OPDOS are used to determine the corresponding bond strengths.

TABLE III. Charge differences for $CO/Pt_{24}Os_2$, $CO/PtOs_4$, and $CO/Pt_{22}Ru_2Os_2$ alloys relative to CO/Pt_{26} for the CO contribution to the adsorbate $4\tilde{\sigma}$, $5\tilde{\sigma}$, $1\tilde{\pi}$, $\tilde{d}_{\pi}$, $\tilde{d}_{\sigma}$, and the occupied part of the $2\tilde{\pi}^*$ orbitals per carbon and oxygen atom. These values are calculated by AOMIX program via DOS integration in the appropriate energy regions.

	Substrate					
	$Pt_{24}Os_2$		$Pt_{22}Os_4$		$Pt_{22}Ru_2Os_2$	
CO contribution	C	O	C	O	C	O
$4\tilde{\sigma}$	0.014	−0.001	0.018	−0.019	0.007	<−0.001
$5\tilde{\sigma}$	<0.001	−0.017	−0.005	0.003	0.004	−0.008
$\tilde{d}_{\sigma}$	−0.013	0.007	−0.012	0.005	0.016	0.006
$1\tilde{\pi}$	0.002	−0.006	0.005	−0.039	0.005	−0.053
$\tilde{d}_{\pi}$	−0.001	0.003	0.004	0.009	0.009	0.037
$2\tilde{\pi}^*$	−0.002	0.012	−0.001	−0.001	0.010	−0.005

The observed charge increase in the CO region of the $4\tilde{\sigma}$ orbital for $CO/Pt_{24}Os_2$ relative to CO/Pt_{26} (Table I) is mostly due to a charge increase in the carbon region of the orbital, accompanied by minimal charge decrease in the oxygen region of the orbital (Table III). The increased charge in the CO region of the $4\tilde{\sigma}$ orbital is indicative of reduced 4σ donation to the metal substrate bands, which weakens both the CO_{ads} internal bond and the C–Pt bond. Moreover, the increased polarization towards carbon further weakens the CO_{ads} internal bond and diminishes the weakening of the C–Pt bond caused by the $4\tilde{\sigma}$ charge changes in the orbital's CO region. The C–Pt OPDOS for the $4\tilde{\sigma}$ orbital between the two systems examined here is reduced by 0.005, thus indicating a weaker C–Pt bond. Nilsson and Pettersson interpreted the increased $4\tilde{\sigma}$ polarization towards carbon as increased C–O anti-bonding due to the increased population of the carbon 2*s* orbital.[47] Our calculations verify that for $CO/Pt_{24}Os_2$-$4\tilde{\sigma}$ relative to CO/Pt_{26}-$4\tilde{\sigma}$ the carbon 2*s* contribution to the $4\tilde{\sigma}$ orbital is increased.

The CO contribution to the $5\tilde{\sigma}$ orbital is reduced for $CO/Pt_{24}Os_2$ relative to CO/Pt_{26}. In general, for CO adsorbed on the nanoclusters of this work, an increased CO contribution to the $4\tilde{\sigma}$ orbital is accompanied by a reduced CO contribution to the $5\tilde{\sigma}$ orbital and vice versa. The observed charge reduction in the CO region of the $5\tilde{\sigma}$ orbital is mainly due to a charge reduction in the oxygen region of the orbital, which reduces the orbital polarization towards oxygen (the carbon 2*s* population remains constant). The charge reduction in the

oxygen region of the $5\tilde{\sigma}$ orbital strengthens the CO_{ads} internal bond, while minimally affects the C–Pt bond. Figure 6 (upper graph) shows that the $\tilde{d}_{\sigma}$-band affects both the CO_{ads} internal bond and the C–Pt bond. Therefore, in this work we consider the changes on the carbon 2*s* population of the whole $\tilde{\sigma}$-system as the determining factor for the relative strength of the CO_{ads} internal bond. For $CO/Pt_{24}Os_2$ relative to CO/Pt_{26} the overall carbon 2*s* population is increased: Therefore, the $CO/Pt_{24}Os_2$-$\tilde{\sigma}$ relative to CO/Pt_{26}-$\tilde{\sigma}$ weakens the CO_{ads} internal bond.

Charge reduction in the CO region of the $CO/Pt_{24}Os_2$-$\tilde{d}_{\sigma}$ relative to CO/Pt_{26}-$\tilde{d}_{\sigma}$ is indicative of stronger C–Pt bond. However, this effect does not counterbalance the C–Pt weakening caused by changes in the $4\tilde{\sigma}$ orbital for $CO/Pt_{24}Os_2$ relative to CO/Pt_{26} as described above. Moreover, the increased population on the Pt^c-*sp* and -d_{z^2} orbitals further weakens the C–Pt bond. Therefore, the $CO/Pt_{24}Os_2$-$\tilde{\sigma}$ system also weakens the C–Pt bond relative to CO/Pt_{26}-$\tilde{\sigma}$. The relative strengths on the CO_{ads} and C–Pt bonds drawn from variations in the $\tilde{\sigma}$-system here are in agreement with prior calculations using periodic DFT.[35]

b. $\tilde{\pi}$-system. For $CO/Pt_{24}Os_2$ relative to CO/Pt_{26} the charge in the CO region of the $1\tilde{\pi}$ orbital is reduced (Table I). This effect corresponds to charge reduction in the oxygen region of the $1\tilde{\pi}$ orbital accompanied by charge increase in the carbon region of the orbital (i.e., the $1\tilde{\pi}$ orbital polarization towards oxygen is reduced). Changes in the CO contribution of the $CO/Pt_{24}Os_2$-$1\tilde{\pi}$ relative to CO/Pt_{26}-$1\tilde{\pi}$ *and* in the polarization of the $1\tilde{\pi}$ orbital weaken the CO_{ads} internal bond. Moreover, the increased carbon population of the $1\tilde{\pi}$ orbital strengthens the C–Pt bond. These results are in agreement with corresponding C–O and C–Pt OPDOS calculations. More specifically, for $CO/Pt_{24}Os_2$-$1\tilde{\pi}$ relative to CO/Pt_{26}-$1\tilde{\pi}$ the C–O OPDOS is reduced by 0.004, while the C–Pt OPDOS is increased by 0.006. For $CO/Pt_{24}Os_2$-$\tilde{d}_{\pi}$ relative to CO/Pt_{26}-$\tilde{d}_{\pi}$, minimal charge change is observed in the carbon region of the orbital, which is indicative of a constant CO_{ads} internal bond (Table III). Finally, charge is increased in the CO region of the $CO/Pt_{24}Os_2$-$2\tilde{\pi}^*$ relative to CO/Pt_{26}-$2\tilde{\pi}^*$, concomitant with reduced orbital polarization towards carbon. The former observation is indicative of weaker CO_{ads} internal bond, while the latter observation indicates the exact opposite effect on the same bond. Minimal changes in the populations and polarizations in the tilde-type orbitals obtained through DOS integration cannot sometimes determine the final effect of the orbitals on the CO_{ads} and C–Pt bonds. The C–O OPDOS shows that $CO/Pt_{24}Os_2$-$2\tilde{\pi}^*$ strengthens both the CO_{ads} and the C–Pt bonds relative to CO/Pt_{26}-$2\tilde{\pi}^*$(C–O and C–Pt OPDOS increase by 0.005 and 0.021, respectively).

For the systems of this work the overall charge change in the carbon region of the $\tilde{\pi}$-system is indicative of the CO_{ads} internal bond relative strength. The carbon population in the $\tilde{\pi}$-system for $CO/Pt_{24}Os_2$ relative to CO/Pt_{26} changes is constant (i.e., the $\tilde{\pi}$-system does not affect the CO_{ads} internal bond). This result is verified by the approximately constant C–O OPDOS for $CO/Pt_{24}Os_2$ relative to CO/Pt_{26} (C–O OPDOS difference within 0.001). Here, the $\tilde{\pi}$-system strengthens the C–Pt bond mostly use to the above changes in the $2\tilde{\pi}^*$ orbital. The weakening of the CO_{ads} and C–Pt bonds, for $CO/Pt_{24}Os_2$ relative to CO/Pt_{26}, is due to changes in the $\tilde{\sigma}$-system as described in Subsection III B 3 a. We need to mentioned here that changes in the overall $\tilde{\pi}$-system as described in this subsection are in partial agreement with the prior corresponding calculation using periodic DFT (i.e., almost invariant CO_{ads} internal bond and weaker C–Pt bond). This outcome is indicative of the different behavior between the cluster and periodic DFT calculations and has been previously reported.[39]

4. CO adsorbed on the $Pt_{22}Os_4$ nanocluster

a. $\tilde{\sigma}$-system. As the Os mole percent in the PtOs alloy increases (i.e., $CO/Pt_{22}Os_4$ nanocluster) the CO contributions to the $4\tilde{\sigma}$ and $5\tilde{\sigma}$ orbital revert to about the same values as the ones observed for the CO/Pt_{26} cluster (Table I). The overall carbon 2*s* population of the $\tilde{\sigma}$-system is approximately constant as the Os mole percent in the PtOs alloy increases, which is indicative of an invariant CO_{ads} internal bond due to changes in the $\tilde{\sigma}$-system. The increased Os mole percent in the PtOs alloy increases the overall charge in the Pt^c-*sp* and -d_{z^2} orbitals leading to a weaker C–Pt bond. Therefore, changes in the $\tilde{\sigma}$-system strengthen the C–Pt bond following the substrate trend $Pt_{26} > Pt_{24}Os_2 > Pt_{22}Os_4$.

b. $\tilde{\pi}$-system. The CO contribution to the $CO/Pt_{22}Os_4$ -$1\tilde{\pi}$ reduces relative to $CO/Pt_{24}Os_2$ -$1\tilde{\pi}$, thus weakening the CO_{ads} internal bond and strengthening the C–Pt bond. These statements are in agreement with the C–O and C–Pt OPDOS observed changes by -0.003 and $+0.006$, respectively. The observed charge reduction in the CO region of the $1\tilde{\pi}$ orbital, as the Os mole percent in the PtOs nanocluster alloy is increased, is in agreement with corresponding calculations under periodic DFT. As the Os mole percent on the PtOs alloy is increased, the C–Pt bond weakening caused by changes in the $\tilde{d}_{\pi}$ and the $2\tilde{\pi}^*$ orbitals does not counterbalance the strengthening caused by changes in the $1\tilde{\pi}$, thus leading to a stronger C–Pt bond (C–Pt OPDOS increases by 0.004). Concomitantly, the overall carbon charge change for the $\tilde{\pi}$-system orbitals is increasing and is indicative of CO_{ads} internal bond weakening. Changes in the $\tilde{\pi}$-system strengthen the C–Pt bond following the substrate trend $Pt_{24}Os_4 > Pt_{22}Os_2 > Pt_{26}$.

5. CO adsorbed on the $Pt_{22}Ru_2Os_2$ nanocluster

a. $\tilde{\sigma}$-system. For $CO/Pt_{22}Ru_2Os_2$ relative to $CO/Pt_{22}Os_4$, the overall carbon 2*s* population for the $\tilde{\sigma}$ system is increased, which is indicative of CO_{ads} internal bond weakening. Here, the C–Pt bond strengthens mostly due to the substantial reduction of the overall charge in the Pt^c-*sp* and -d_{z^2} orbitals. The strengthening of the C–Pt bond is in contrast to what was observed from corresponding periodic DFT calculations. However, we must recall that for the periodic DFT calculations the C–Pt bond was found to be weaker for $CO/PtRu_2Os_2$ relative to $CO/PtOs_4$, which is

opposite to what is observed in the corresponding nanocluster calculations of this work. Therefore, in some cases CO adsorption calculations on nanoclusters may not correspond to adsorption on a surface, which is more accurately mimicked by periodic DFT calculations.

b. $\tilde{\pi}$-system. For $CO/Pt_{22}Ru_2Os_2$ relative to $CO/Pt_{22}Os_4$, the $\tilde{\pi}$-system weakens the CO_{ads} internal bond, as evidenced from the increased change in the carbon region of the $\tilde{\pi}$-system. Changes in the $\tilde{\pi}$-system weaken the C–Pt bond for $CO/Pt_{22}Ru_2Os_2$ relative to $CO/Pt_{22}Os_4$, mostly due to the increased change in the CO region of the $\tilde{d}_\pi$ orbital. For $CO/Pt_{22}Ru_2Os_2$ relative to $CO/Pt_{22}Os_4$ a competition between the $\tilde{\sigma}$ and the $\tilde{\pi}$-system strengthens the C–Pt bond (vide infra). The last result is in agreement with increase in the C–Pt OPDOS by 0.017 between the two systems examined here.

IV. COMPARISON OF OUR NEW MODEL WITH THE FRONTIER ORBITAL MODEL

Figure 7 shows the ν_{CO}, the overall charge of the CO contributions to the adsorbate $5\tilde{\sigma}$ orbital and the occupied part of the $2\tilde{\pi}^*$ orbital, the net effect of the carbon $2s$ part of the $\tilde{\sigma}$-system and the carbon p_{xy} part of the $\tilde{\pi}$-system for CO adsorbed on Pt_{26}, $Pt_{24}Os_2$, $Pt_{22}Os_4$, and $Pt_{22}Ru_2Os_2$ nanoclusters. We recall that the CO contribution to the adsorbate $5\tilde{\sigma}$ orbital is related to the charge donated from the adsorbate to the metal bands, whereas the corresponding contribution to the occupied part of the $2\tilde{\pi}^*$ orbital is related to the back-donated charge from the metal bands to the CO_{ads} (frontier orbital model). In our last report, we found that the frontier orbital model is not sufficient to describe changes on the CO_{ads} internal bond and the C–Pt bond as Pt is alloyed with Ru/Os atoms. This result is also confirmed here, as Figs. 7(a) and 7(b) show no trend between the net charge in the CO region of the $5\tilde{\sigma}$ and $2\tilde{\pi}^*$ orbitals and the ν_{CO} for the systems of this work. However, the net charge of the carbon $2s$ and p_{xy} orbitals as discussed above increases as ν_{CO} reduces, and thus can be used as an indicator for the relative CO_{ads} internal bond strength.

For the systems of this work, Figure 8 reveals a trend between the ν_{CPt} and the algebraic summation of the following charges (model for C–Pt bond strength): the CO contributions

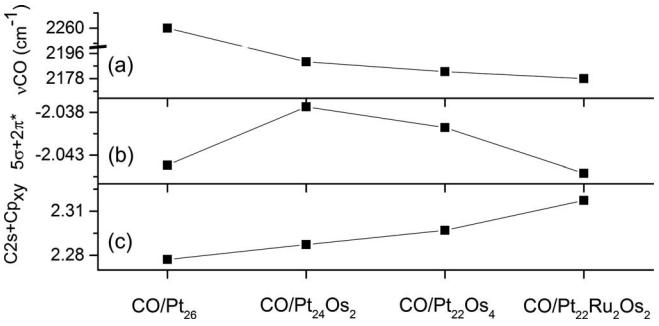

FIG. 7. (a) ν_{CO}, (b) overall charge of the CO contributions to the adsorbate $5\tilde{\sigma}$ and $2\tilde{\pi}^*$ orbitals (occupied part), (c) combined effect of the carbon $2s$ (C$2s$) part of the $\tilde{\sigma}$-system and the carbon p_{xy} (Cp_{xy}) part of the $\tilde{\pi}$-system for CO/Pt_{26}, $CO/Pt_{24}Os_2$, $CO/Pt_{22}Os_4$, and $CO/Pt_{22}Ru_2Os_2$.

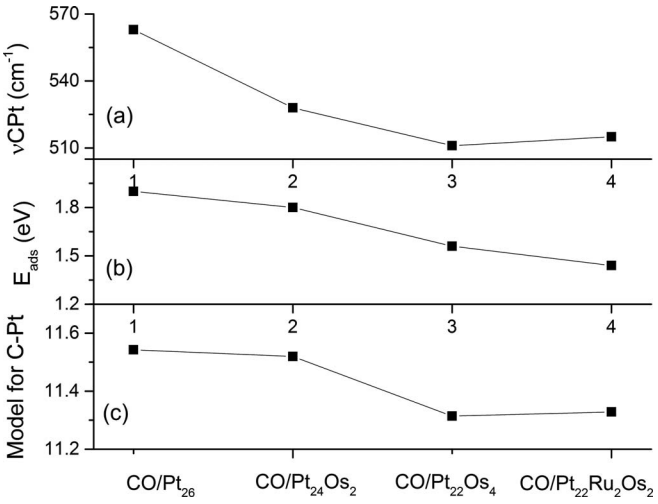

FIG. 8. (a) ν_{CPt}, (b) E_{ads}, and (c) overall charge of the CO contributions to the adsorbate-tilde orbitals using the phenomenological model for C–Pt bond strength prediction for CO/Pt_{26}, $CO/Pt_{24}Os_2$, $CO/Pt_{22}Os_4$, and $CO/Pt_{22}Ru_2Os_2$.

to the $4\tilde{\sigma}$, $5\tilde{\sigma}$, $1\tilde{\pi}$, and $2\tilde{\pi}^*$ orbitals and the atomic populations of the Pt^c $d_{xz,\,yz}$ and $d_{x^2-y^2}$ orbitals, which contribute to C–Pt bonding, with the negative of the atomic populations of the Pt^c-sp and -d_{z^2} orbital and the negative of the charge $\tilde{d}_\sigma$ and $\tilde{d}_\pi$ bands, which contribute to C–Pt anti-bonding. The relative strength of the C–Pt bond is well correlated with changes in the CO contribution of the $\tilde{\sigma}$ and $\tilde{\pi}$ system orbitals and the Pt^c atomic orbitals.

The downshift of the d-band center for $CO/Pt_{24}Os_2$ relative to CO/Pt_{26} (Fig. 3) suggests less overlap of the $2\tilde{\pi}^*$ with the substrate bands, and thus stronger CO_{ads} internal bond. However, this is not the case here: The CO_{ads} internal bond weakens as Pt is alloyed with Os atoms (ν_{CO} reduction, Table I). In general, the d-band center argument by Hammer *et al.*[41] cannot be used to correctly predict the relative strength of the CO_{ads} internal bond for the systems of this work. This statement is in agreement with our prior calculations under periodic DFT.

V. CONCLUSIONS

DFT spin-optimized calculations for CO adsorbed on Pt_{26}, $Pt_{24}Os_2$, $Pt_{22}Os_4$, and $Pt_{22}Ru_4Os_4$ nanoclusters have been employed to develop a new phenomenological model, which relates the CO_{ads} internal bond strength with the polarization of the $\tilde{\sigma}$ and $\tilde{\pi}$ system orbitals. Our methodology was inspired by the original and $\tilde{\pi}$-$\tilde{\sigma}$ model of Nilsson and coworkers,[42,44–47] with the inclusion of the σ donation part. The traditional model of 5σ-donation to the metal bands and 2π*-back donation was found insufficient to explain changes in the CO_{ads} internal bond the C–Pt bond as the Pt_{26} nanocluster was alloyed by Ru/Os atoms. The DFT calculated ν_{CO} and ν_{CPt} on the above nanoclusters are used as a relative measure of the CO_{ads} internal bond strength and the C–Pt bond strength, respectively. For the CO_{ads} internal bond strength, a trend is drawn between ν_{CO} and the net charge of the carbon $2s$ ($\tilde{\sigma}$ polarization) and p_{xy} ($\tilde{\pi}$ polarization) atomic orbital populations. This result is in agreement with prior periodic DFT

calculations on corresponding Pt, PtOs, and $PtRu_2Os_2$ slabs. Concomitantly, for the C–Pt bond strength, we presented an empirical model that relate the ν_{CPt} with the CO contributions of the $\tilde{\sigma}$ and $\tilde{\pi}$ system orbitals and the Pt^c -*sp* and -*d* orbital populations.

ACKNOWLEDGMENTS

Funding was provided by the UTPA-FRC grant. Calculations were performed using the High Performance Computing Cluster at the University of Texas-Pan American.

[1]M. Watanabe, M. Vehida, and S. Motoo, J. Electroanal. Chem. **229**, 395–406 (1987).
[2]A. Hamnet and B. J. Kennedy, Electrochim. Acta **33**, 1613–1618 (1988).
[3]G. L. Troughton and A. Hamnett, Bull. Electrochem. **7**, 488–492 (1991).
[4]H. A. Gasteiger, N. Markovic, P. N. Ross, and E. J. Cairns, J. Phys. Chem. **97**, 12020–12029 (1993).
[5]E. Herrero, K. Franaszczuk, and A. Wieckowski, J. Electroanal. Chem. **361**, 269–273 (1993).
[6]M. Krausa and W. Vielstich, J. Electroanal. Chem. **379**, 307–314 (1994).
[7]H. A. Gasteiger, N. Markovic, and P. N. Ross, J. Phys. Chem. **99**, 16757–16767 (1995).
[8]M. P. Hogarth and G. A. Hards, Platinum Met. Rev. **40**, 150–159 (1996).
[9]T. Frelink, W. Visscher, and J. A. R. van Veen, Langmuir **12**, 3702–3708 (1996).
[10]K. L. Ley, R. Liu, C. Pu, Q. Fan, N. Leyarovska, C. Segre, and E. S. Smotkin, J. Electrochem. Soc. **144**, 1543–1548 (1997).
[11]W. Chrzanowski and A. Wieckowski, Langmuir **13**, 5974–5978 (1997).
[12]W. Chrzanowski, H. Kim, and A. Wieckowski, Catal. Lett. **50**, 69–75 (1998); W. Chrzanowski, H. Kim, G. Tremiliosi-Filho, A. Wieckowski, B. Grzybowska, and P. Kulesza, J. New Mater. Electrochem. Syst. **1**, 31–38 (1998).
[13]E. Reddington, A. Sapienza, B. Gurau, R. Viswanathan, S. Sarangapani, E. S. Smotkin, and T. Mallouk, Science **280**, 1735–1737 (1998).
[14]A. B. Anderson, E. Grantscharova, and S. Seong, J. Electrochem. Soc. **143**, 2075–2082 (1996).
[15]M. Watanabe and S. Motoo, J. Electroanal. Chem. **60**, 267–273 (1975).
[16]A. Kabbabi, R. Faure, R. Durand, B. Beden, F. Hahn, J.-M. Leger, and C. Lamy, J. Electroanal. Chem. **444**, 41–53 (1998).
[17]M. J. Gonzalez, C. T. Hable, and M. S. Wrighton, J. Phys. Chem. B **102**, 9881–9890 (1998).
[18]T. Frelink, W. Visscher, A. P. Cox, and J. A. R. Van Veen, Electrochim. Acta **40**, 1537–1543 (1995).
[19]R. Liu, H. Iddir, Q. Fan, G. Hou, A. Bo, K. L. Ley, E. S. Smotkin, Y. E. Sung, H. Kim, S. Thomas, and A. Wieckowski, J. Phys. Chem. B **104**, 3518–3531 (2000).
[20]Y. Ishikawa, M. S. Liao, and C. R. Cabrera, Surf. Sci. **513**, 98–110 (2002).
[21]Y. Y Tong, H. S. Kim, P. K. Babu, P. Waszczuk, A. Wieckowski, and E. Oldfield, J. Am. Chem. Soc. **124**, 468–473 (2002).
[22]B. R. Rauhe, F. R. McLarnon, Jr., and E. J. Cairns, J. Electrochem. Soc. **142**, 1073–1084 (1995).
[23]J. O'M. Bockris and H. Wroblowa, J. Electroanal. Chem. **7**, 428–451 (1964).
[24]B. Beden, C. Lamy, A. Bewick, and K. Kunimatsu, J. Electroanal. Chem. **121**, 343–347 (1981).
[25]A. O. Petrii and V. D. Kalinin, Russ. J. Electrochem. **35**, 699–707 (1999).
[26]A. Crown, I. R. Moraes, and A. Wieckowski, J. Electroanal. Chem. **500**, 333–343 (2001).
[27]G. Orozco and C. Gutiérrez, J. Electroanal. Chem. **484**, 64–72 (2000).
[28]Y. Zhu and C. R. Cabrera, Electrochem. Solid-State Lett. **4**, A45–A48 (2001).
[29]E. I. Santiago, M. J. Giz, and E. A. Ticianelli, J. Solid State Electrochem. **7**(9), 607–613 (2003).
[30]N. Dimakis, H. Iddir, R. R. Diaz-Morales, R. Liu, G. Bunker, E. H. Chung, and E. S. Smotkin, J. Phys. Chem. B **109**, 1839–1848 (2005).
[31]A. Baro and H. Ibach, J. Chem. Phys. **71**, 4812–4816 (1979).
[32]H. Steininger, S. Lehwald, and H. Ibach, Surf. Sci. **123**, 264–282 (1982).
[33]L.-W. H. Leung, S.-C. Chang, and M. J. Weaver, J. Chem. Phys. **90**(14), 7426–7436 (1989).
[34]Y. Gauthier, M. Schmid, S. Padovani, E. Lundgren, V. Bus, G. Kresse, J. Redinger, and P. Varga, Phys. Rev. Lett. **87**(3), 036103 (2001).
[35]N. Dimakis, T. Mion, and E. S. Smotkin, J. Phys. Chem. C **116**(40), 21447–21458 (2012).
[36]G. Blyholder, J. Phys. Chem. **68**, 2772–2778 (1964).
[37]P. S. Bagus and G. Pacchioni, Surf. Sci. **278**, 427–436 (1992).
[38]S. S. Sung and R. Hoffmann, J. Am. Chem. Soc. **107**, 578–584 (1985).
[39]N. Dimakis, M. Cowan, G. Hanson, and E. S. Smotkin, J. Phys. Chem. C **113**(43), 18730–18739 (2009).
[40]B. Hammer and J. K. Nørskov, Nature (London) **376**, 238–240 (1995).
[41]B. Hammer, Y. Morikawa, and J. K. Nørskov, Phys. Rev. Lett. **76**, 2141–2144 (1996).
[42]A. Nilsson, M. Weinelt, T. Wiell, P. Bennich, O. Karis, and N. Wassdahl, Phys. Rev. Lett. **78**, 2847–2850 (1997).
[43]P. Bennich, T. Wiell, O. Karis, M. Weinelt, N. Wassdahl, A. Nilsson, M. Nyberg, L. G. M. Pettersson, J. Stöhr, and M. Samant, Phys. Rev. B **57**, 9274–9284 (1998).
[44]A. Föhlisch, M. Nyberg, J. Hasselström, O. Karis, L. G. M. Pettersson, and A. Nilsson, Phys. Rev. Lett. **85**, 3309–3312 (2000).
[45]A. Föhlisch, M. Nyberg, P. Bennich, L. Triguero, J. Hasselström, O. Karis, L. G. M. Petterssonm, and A. Nilsson, J. Chem. Phys. **112**, 1946–1958 (2000).
[46]A. Föhlisch, J. Hasselström, P. Bennich, N. Wassdahl, O. Karis, A. Nilsson, L. Triguero, M. Nyberg, and L. G. M. Pettersson, Phys. Rev. B **61**, 16229–16240 (2000).
[47]A. Nilsson and L. G. M. Pettersson, Surf. Sci. Rep. **55**, 49–167 (2004).
[48]G. Kresse, A. Gil, and P. Sautet, Phys. Rev. B **68**, 073401 (2003).
[49]G. Rangelov, N. Memmel, E. Bertel, and V. Dose, Surf. Sci. **251–252**, 965–970 (1991).
[50]H. Aizawa and S. Tsuneyuki, Surf. Sci. **399**, L364–L370 (1998).
[51]P. Hohenberg and W. Kohn, Phys. Rev. **136**, B864–B871 (1964).
[52]W. Kohn and L. J. Sham, Phys. Rev. **137**, A1697–A1705 (1965).
[53]R. G. Parr and W. Yang, *Density Functional Theory of Atoms and Molecules* (Oxford University Press, New York, 1989).
[54]X. Xu and W. A. Goddard, Proc. Natl. Acad. Sci. U.S.A. **101**, 2673–2677 (2004).
[55]X. Xu, Q. Zhang, R. Muller, and W. A. Goddard, J. Chem. Phys. **122**, 014105 (2005).
[56]A. D. Becke, J. Phys. Chem. **98**, 5648–5652 (1993).
[57]J. Jacob and W. A. Goddard, J. Phys. Chem. B **108**, 8311–8323 (2004).
[58]M. J. Frisch, J. A. Pople, and J. S. Binkley, J. Chem. Phys. **80**, 3265–3269 (1984).
[59]T. Clark, J. Chandrasekhar, G. W. Spitznagel, and P. V. R. Schleyer, J. Comput. Chem. **4**, 294–301 (1983).
[60]Inclusion of the outermost core electrons with the valence electron is necessary because theses core orbitals have similar size as the valence electrons.
[61]P. J. Hay and W. R. Wadt, J. Chem. Phys. **82**, 299–310 (1985).
[62]W. J. Hehre, L. Radom, P. V. R. Schleyer, and J. A. Pople, *Ab initio Molecular Orbital Theory* (Willey, New York, 1987).
[63]S. I. Gorelsky, *AOMix: Program for Molecular Orbital Analysis* (University of Ottawa, 2007), see http://www.sg-chem.net/.
[64]S. F. Boys and F. Bernardi, Mol. Phys. **19**, 553–566 (1970).
[65]Jaguar 7.7, Schrodinger Inc., Portland, OR.
[66]R. Friesner, Chem. Phys. Lett. **116**, 39–43 (1985).
[67]R. Friesner, J. Chem. Phys. **86**, 3522–3531 (1987).
[68]R. Friesner, J. Chem. Phys. **85**, 1462–1468 (1986).
[69]M. N. Ringnalda, Y. Won, and R. Friesner, J. Chem. Phys. **92**, 1163–1173 (1990).
[70]J. M. Langlois, P. R. Muller, T. R. Coley, W. A. Goddard, M. N. Ringnalda, Y. Won, and R. Friesner, J. Chem. Phys. **92**, 7488–7497 (1990).
[71]M. N. Ringnalda, M. Belhadj, and R. Friesner, J. Chem. Phys. **93**, 3397–3407 (1990).
[72]E. D. Glendening, J. K. Badenhoop, A. E. Reed, J. E. Carpenter, J. A. Bohmann, C. M. Morales, and F. Weinhold, *NBO 5.0* (Theoretical Chemistry Institute, University of Wisconsin, Madison, WI, 2001).
[73]S. I. Gorelsky and A. B. P. Lever, J. Organomet. Chem. **635**, 187–196 (2001).

[74]A. P. Scott and L. J. Radom, Phys. Chem. **100**, 16502–16513 (1996).
[75] M. T. Koper, T. E. Shubina, and R. A. van Santen, J. Phys. Chem. B **106**, 686–692 (2002).
[76]J. Kua and W. A. Goddard III, J. Phys. Chem. B **102**, 9481–9500 (1998).
[77]J. Kua and W. A. Goddard III, J. Am. Chem. Soc. **121**, 10928–10941 (1999).
[78]See supplementary material at http://dx.doi.org/10.1063/1.4802817 for the partial charges per layer for the clean substrates in this work.